JOURNAL OF MATERIALS SCIENCE **38** (2003) 705–712

Microstructure, electrochemical surface and electrocatalytic properties of $IrO_2+Ta_2O_5$ oxide electrodes

JI-MING HU, JIAN-QING ZHANG*
Chemistry Department, Zhejiang University, Hangzhou 310027, People's Republic of China
E-mail: zjq@public1.zju.edu.cn

HUI-MIN MENG
Beijing Corrosion and Protection Center, University of Science and Technology Beijing, Beijing 100083, People's Republic of China

CHU-NAN CAO
Chemistry Department, Zhejiang University, Hangzhou 310027, People's Republic of China

X-ray diffraction (XRD) and scanning electron microscopy (SEM) have been used to characterize physical structure of $IrO_2+Ta_2O_5$ films over the whole composition range by thermodecomposition of chloride solutions heated at 450°C. Solid solubilization between Ta component and IrO_2 rutile in the mixed films was measured, and three typical surface morphologies of the oxide coatings were observed. The surface electrochemical properties of Ti/IrO_2-Ta_2O_5 electrodes were studied by cyclic voltammetry at varying potential scan rate, and a 'double-layer' electrochemical structure containing the 'inner' and 'outer' layers has been distinguished. The voltammetric charge appears to decline with the decrease of grain size of oxide coatings as a result of the effect of surface tension. However, the coatings of 70% IrO_2+30% Ta_2O_5 with the finest grains still exhibit the highest apparent activity for oxygen evolution evaluated by the anodic current at a constant potential. This result is interpreted by the measurements of open-circuit potential (E_{oc}) and double-layer capacitance (C_{dl}) using electrochemical impedance spectroscopy (EIS). Thereby, the reliability of voltammetric charge obtained in 'double-layer' potential region in determining the real electrocatalytic activity for O_2 evolution has been discussed.

1. Introduction

Ti based oxide coating electrodes have been extensively studied since the past 30 years [1, 2]. An interest in IrO_2 as the electrocatalyst for O_2 evolution in acidic media has been shown [3, 4]. In binary systems, the combination of active IrO_2 and inert Ta_2O_5 exhibits good performance in anodic stability and electrocatalytic activity [5–7].

Rogiskaya *et al.* [8, 9] systematically investigated the microstructure of $IrO_2+Ta_2O_5$ coatings, and the formation of solid solution between the two oxides has been observed. In our previous work [10], the crystalline orientation of IrO_2 rutile and its effect on corrosion characteristics of Ta_2O_5 mixed active anodes have been reported. Studies on electrocatalytic activity and durability of this type of anode have been extensively carried out by Comninellis and his co-workers [5–7, 11, 12]. Nevertheless, intensive works on the structure dependence of anode properties have not been sufficiently investigated in the previous literatures [4, 13]. For instance, it is well known that coatings of IrO_2 (70 mol%) + Ta_2O_5 (30 mol%) display the highest activity for O_2 evolution [5, 12], however there is no definite interpretation for this phenomenon. An apparently electrocatalytic activity of oxide anodes for gas evolution can be reasonably determined by the anodic current at a certain potential (or by the potential at a certain current) in E-logi curves. As a common method for active surface area determination, the integrated charge from voltammetric curves was employed [14, 15]. However, it should be noted that, the voltammetric curves for charge integration is operated in a potential window avoiding the hydrogen and oxygen evolution (i.e. so-called 'double-layer' potential region), whilst the practical oxygen evolution is taken place at a relatively higher potential. After attacked by the gas bubbling, the porous surface tends to be modified, and the active surface area is changed. Therefore, the voltammetric charge obtained at double-layer region potential probably can not preciously reveal the

*Author to whom all correspondence should be addressed.

real active surface area in the case of practical O_2 evolution.

In the present paper, the microstructure, surface morphology and the electrocatalytic properties of the Ti based Ir/Ta mixed oxide anodes were investigated, and the relationship among the above aspects was emphasized. In addition, the reliability of practically electrocatalytic activity determination by voltammetric charge obtained at 'double-layer' potential region for O_2 evolution was also discussed.

2. Experimental details

2.1. Preparation of electrodes

The thermo-decomposition method was used to prepare the oxide coatings. Prior to use, titanium plate (TA1) was degreased, and etched in 3.0 mol dm^{-3} HCl solution, then rinsed with deionized water. The precursors were prepared by mixing appropriate amounts of $H_2IrCl_6 \cdot 6H_2O$ (in hydrochloric acid) solution and $TaCl_5$ (solved in alcohol) solution. As reported by several authors [17, 18], oxide anodes prepared from organic solvent system displayed better performance. In the present work, the mixed chlorides were pre-dried at 80°C for 24 h, then was mechanically powdered. After that, the obtained products were dissolved in 1:1 volume ratio alcohol and isopropanol solutions in which the total metal concentration was kept around 0.2 mol dm^{-3}. Then the Ti substrates were painted with the coating solution by brushes. After being dried at 100°C, the samples were heated at an annealing temperature (450°C) for 10 min. The entire procedure was repeated for 10 times, after which the samples were heated at the annealing temperature for 1 hour. The total loading of the obtained oxide coating was around 10 g m^{-2}.

2.2. Material characterization

X-ray diffraction (XRD) was used to analyze the structure of coatings. The inspection was carried out on a D/MAX-R3 type diffractometer equipped with Cu-Kα radiation and nickel filter. The goniometer was 2° min^{-1}. The crystallite size was calculated on the basis of the Scherrer method [19]. SEM micrographs and EDX spectra were obtained with a Cambridge S-360 Scanning Electron Microscope equipped with a Link Analytical QX2000 X-ray energy dispersive analyzer. A 20 keV electron beam was used.

2.3. Electrochemical analysis

PAR instrumentation was used throughout. All the electrochemical measurements were operated by using three-compartment all-glass cell. A platinum plate was used as the counter electrode, and KCl saturated calomel electrode (SCE) as the reference. The 'standard' voltammetric curves were recorded between 0.16 and 1.16 V (vs. SCE) at 20 mV s^{-1}. The voltammetric charge, q^*, was obtained by graphical integration. As a function of scan rate, the voltammetric curves were obtained at the following sweep rates: 2, 5, 10, 20, 50, 100, 200, and 500 mV s^{-1}. The current-potential curves were recorded by moving the potential anodically in 20 mV step up to 2.0 V (vs. SCE). The current was recorded after 1 min at each potential. The electrochemical impedance spectroscopy (EIS) were conducted in the potentiostatic mode using an EG&G Princeton Applied Research Corp. System (PAR, Model 273) in combination with a phase-sensitive lock-in amplifier (EG&G PAR, Model 5210) for frequency measurements extending from 10 mHz–100 kHz. In EIS measurements two potentials were selected: (i) 0.7 V (SCE), at the 'double-layer' region, and (ii) 1.35 V (SCE), a potential for intensive oxygen evolution reaction (OER). All solution used in this work was 0.5 mol dm^{-3} H_2SO_4 prepared with deionized water. Solution temperature was maintained at 20 ± 0.5°C.

3. Results

3.1. Structure and morphology

XRD patterns (shown in Fig. 1) show both the type and number of crystallite phase vary with the content ratio of Ir/Ta. The peaks of β-Ta_2O_5 appear at 450°C in 100% Ta_2O_5 films, although their intensities are not much strong which is probably associated with the main contribution of broaden amorphous peak. Apart from β-Ta_2O_5, IrO_2 rutile and other undetectable crystallite phases are also identified in 10% IrO_2+Ta_2O_5 and 40% IrO_2+Ta_2O_5 films. The presence of the undetectable phases indicates an incomplete decomposition of the corresponding mixture. A certain amount of amorphous components are presented in the films with IrO_2 mole fraction ≤40% (such as 0%, 10%, and 40%). It is demonstrated that the amount of β-Ta_2O_5 decreases with increasing the content of iridium. As IrO_2 content ≥70%, the crystallite phase in the mixture exists entirely as rutile phase, and none of amorphous peak is detected. This result indicates that the crystallization of Ta_2O_5 is affected by IrO_2 component. Roginskaya *et al.* [8] reported that, in 100% Ta_2O_5 films β-Ta_2O_5 appeared at 450°C, and in Ir/Ta mixed films with 10%

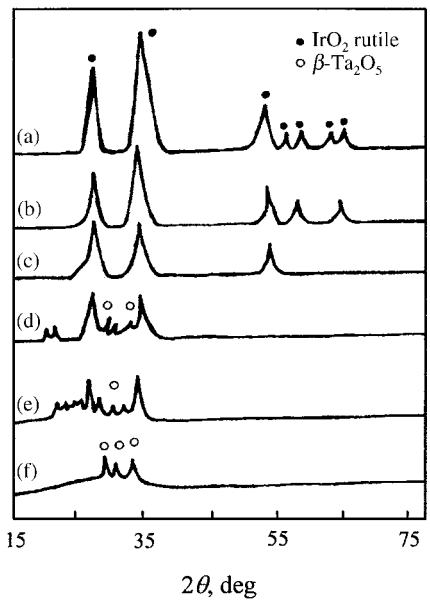

Figure 1 Hand-draft of XRD patterns of Ir/Ta mixed oxide coatings with different compositions (at the pyrolysis temperature of 450°C): (a) 0%, (b) 10%, (c) 40%, (d) 70%, (e) 80%, and (f) 100% IrO_2.

TABLE I Lattice parameters and cell volume of rutile IrO_2 in films x $IrO_2 + (100 - x)$ Ta_2O_5[a]

x (mol%)	T (°C)	a (nm)	c (nm)	V (nm^3)
10	450	0.4554	0.3165	0.0656
26	450	0.4571	0.3132	0.0654
40	450	0.4593	0.3111	0.0656
60	450	0.4560	0.3162	0.0639
70	450	0.4573	0.3185	0.0666
80	450	0.4554	0.3165	0.0656
100	450	0.4561	0.3160	0.0639
	[e]	0.4498	0.3160	0.0639

[a]The calculation of the lattice parameters was made using the (110) and (101) reflections.
[e]Equilibrium lattice parameters of rutile IrO_2 [20].

and 20% IrO_2 it emerged only at 550°C and 650°C, respectively, and complete crystallization of this phase occurred only at 750°C. They also pointed out that, in the binary oxides the β phase was a solid solution of IrO_2 in β-Ta_2O_5. On the other hand, Ta component can also penetrate into IrO_2 rutile crystal by solubilization. The lattice parameters of rutile phase in the films are summarized in Table I. Systematic differences of the parameters with the composition at the same temperature indicate that this phase is a solid solution of Ta component in IrO_2 rutile. Since the ion radius of Ta^{IV}, Ta^{V} and Ir^{IV} are extremely close (0.74, 0.72 and 0.71 Å, respectively [21]), Ir and Ta compounds tend to form a solid solution during the thermolysis formation of the mixed oxides. The rutile lattice is deformed and the cell volume increases due to access of a larger ion of Ta component. As shown in Table I, at 450°C the rutile cell volume of the film with the content of 70% IrO_2 reaches the maximum value, which indicates the maximum solubility of Ta with IrO_2 rutile occurs.

Assuming that only the crystallite size, d, affects the half-peak width, variations of d with composition are obtained by using Scherrer method [91] with the aid of calculation software (shown in Fig. 2). Fig. 2 shows the crystallite size of IrO_2 rutile decreases with the increase of IrO_2 content between 10% and 40%, and increases between 70% and 100%. In the intermediate region, coatings of 60% IrO_2+Ta_2O_5 present a peaked value of d. Two minimum values at 40% and 70% IrO_2 compositions are found over the whole compositional range. This result could be related to the maximum solubility of Ta_2O_5 in IrO_2 rutile for the coatings of 70% IrO_2+Ta_2O_5. Roginskaya and Mororozova [9] reported that, the finer the crystallites of IrO_2, the more the contributions of Ta_2O_5 modification to the mixed modified phase. Therefore, a remarkable effect of Ta component on the crystallization dynamics of IrO_2 crystallite phase is indicated.

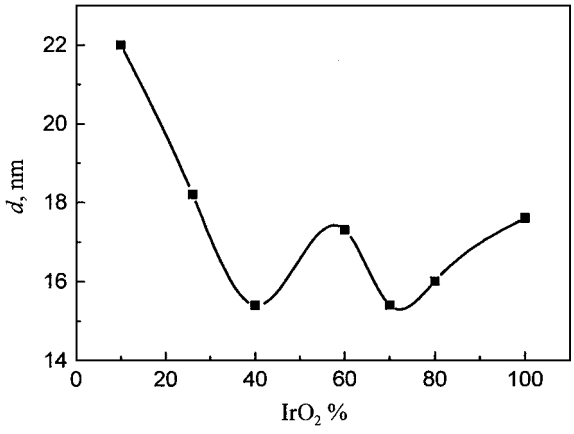

Figure 2 X-ray crystallite size of rutile as a function of IrO_2 content in IrO_2+Ta_2O_5 mixed oxide films.

SEM images show that, in the whole range of composition, coatings display three typical surface features: (1) islands separated by cracks (corresponding to the coatings of 100% Ta_2O_5, and those of 10% and 26% IrO_2+Ta_2O_5); (2) large amount of fine crystallites segregated on the surface of islands (corresponding to the coatings of 40% and 70% IrO_2+Ta_2O_5); and (3) large crystallites segregated on the surface of islands (coatings of 60%, 80% IrO_2+Ta_2O_5 and pure IrO_2). Fig. 3 shows only the typical morphology for each group. The EDX analysis shows a definite evidence of iridium enrichment in the region of the segregated crystallites (See Fig. 4). Based on the XRD patterns, the segregated crystallities on surface can be considered as the enriched IrO_2 rutile. The segregating phenomenon of rutile crystallites suggests that a 'double-layer' physical structure of the oxide coatings be expected. The double-layer electrochemical surface is characterized by cyclic voltammetry measurements (see below). The variation of crystallite size of IrO_2 rutile segregating on surface with composition is much similar to that of the bulk oxides determined by XRD (shown in Fig. 2).

3.2. Open-circuit potential

The open-circuit potential (E_{oc}) in 0.5 mol dm^{-3} H_2SO_4 solutions against the oxide composition of Ti/IrO_2-Ta_2O_5 electrodes is displayed in Fig. 5. E_{oc} increase and then decreases as the IrO_2 content is increased, with a maximum at 70% IrO_2. A similar peaked phenomenon of E_{oc} has been also found in Ti/RuTiCeO$_2$ mixed oxide electrode [22]. This indicates that the surface concentration of active oxide is not simply affected by intimate mixing effect of the inert oxide. Fig. 6 shows the pH dependence of E_{oc} of a mixed oxide electrode containing 70% IrO_2. The experimental data approximately display a straight line with a slop of −0.06 V per unit pH. This result is in agreement with that of a pure IrO_2 sample reported by Ardizzone *et al.* [23].

3.3. Voltammetric charge

Fig. 7 shows one typical voltammetric curve (with 70% IrO_2 content). The voltammetric charge, q^*, obtained by integration of the curves measures the amount of protons exchanged with the solution [24], and peaks in the CV curves are associated with redox transitions of surface sites [25]. The peak observed at c.a. 0.8 V in Fig. 7 has been attributed to the Ir(III)/Ir(IV) transition [26]. Therefore, the value of q^* is expected to be proportional to the number of surface reaction site [27]. The q^* value for the porous electrodes was found to vary with scanning rate, ν [28]. According to the

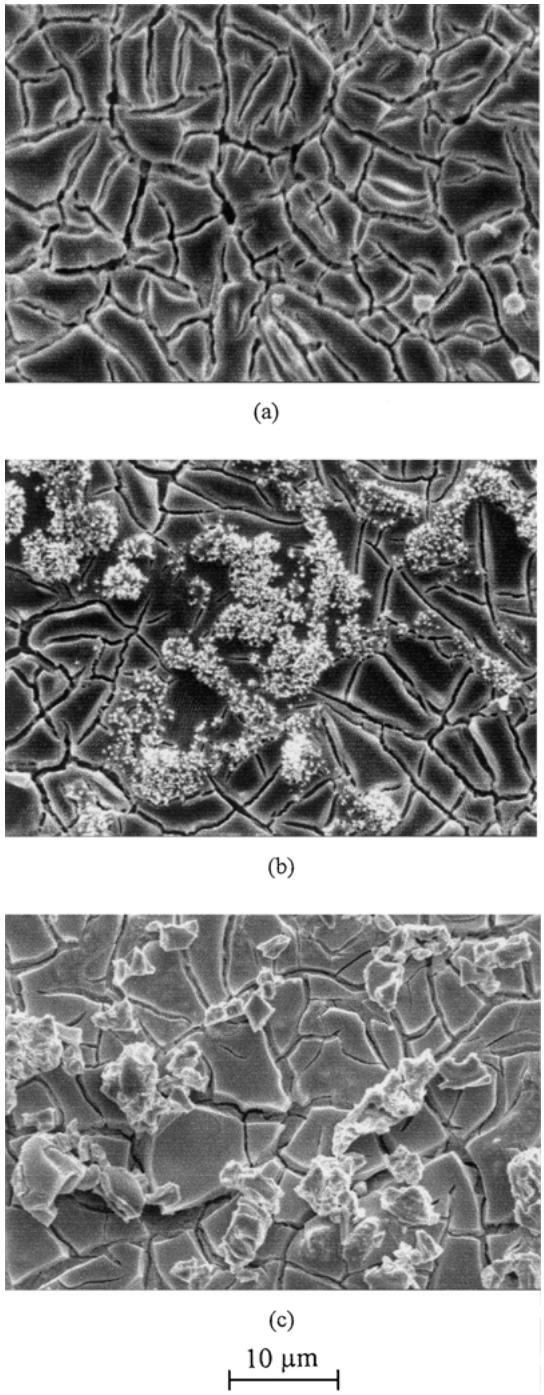

Figure 3 SEM surface images of Ir/Ta oxide coatings with different compositions prepared at 450°C: (a) Ta_2O_5(100%); (b) IrO_2(70%) + Ta_2O_5(30%); (c) IrO_2(100%).

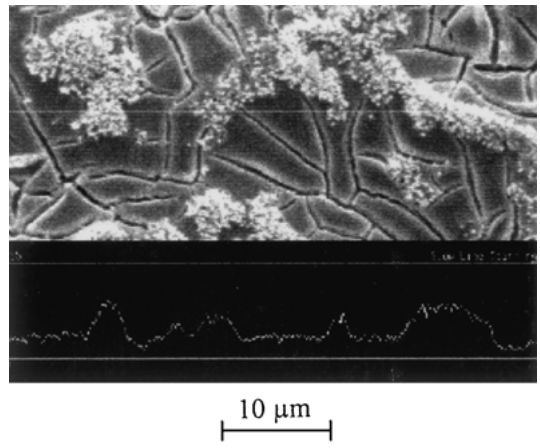

Figure 4 Line scanning profile of Ir element on the surface of Ti/70% IrO_2-30% Ta_2O_5 film.

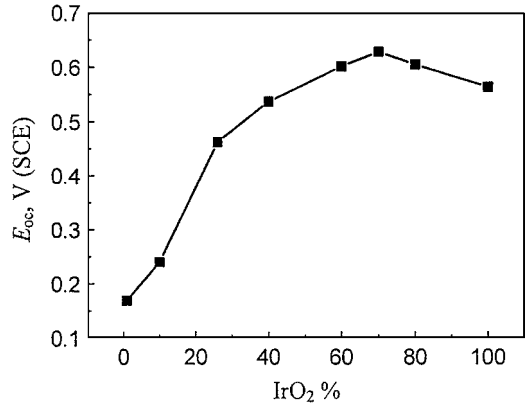

Figure 5 Dependence of open-circuit potential in 0.5 mol dm^{-3} H_2SO_4 solution on the composition of Ti/IrO_2-Ta_2O_5 electrodes.

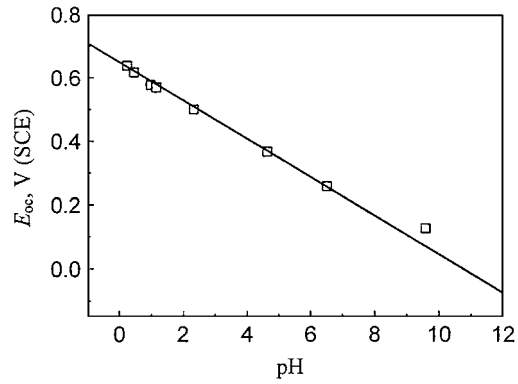

Figure 6 Open-circuit potential vs. pH of the testing solution for a Ti/IrO_2(70%)-Ta_2O_5(30%) mixed oxide electrode. Reading taken after 30 min of immersion.

works carried out by Ardizzone *et al.* [28] and de Pauli and Trasatti (1995), charge of the 'outer' surface, q_s^*, is corresponding to that extrapolated to $\nu = \infty$, while the 'inner' one, q_i^*, is determined as

$$q_i^* = q^*(\nu = 0) - q^*(\nu = \infty) \qquad (1)$$

where $q^*(\nu = 0)$ gives q_T^*, the total charge related to the whole active surface.

Voltammetric charge was normalized by the loading of active oxide in coatings in many previous works [5, 8]. However, because not the total amount of active component makes a contribution to the surface activity of electrodes, a new denotation for voltammetric charge normalized by IrO_2 content (in mole fraction), which is more accurately associated with the charges of unit active site on surface, is employed in this paper. As the examples, determination of $q^*(\nu = 0)$ from the extrapolation of $1/q^*$ to $\nu^{(1/2)} = 0$ for the samples of 26%, 60%, and 70% IrO_2 is displayed in Fig. 8. The plots are approximately linear over the whole range of scan rate. However, the extrapolation of q^* to $\nu^{(-1/2)} = 0$ (to determine $q^*(\nu = \infty)$) is not so ideal (see Fig. 9). In the region of high ν value, q^* is found to decrease rapidly, which has been explained by an uncompensated ohmic

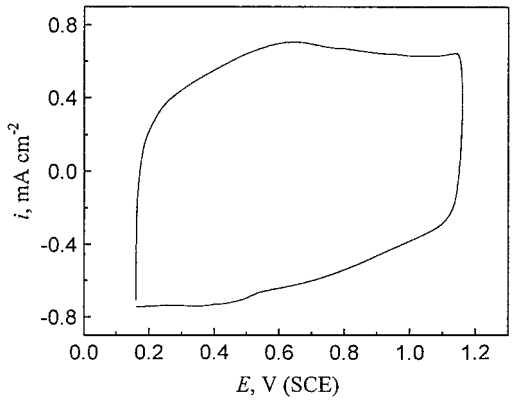

Figure 7 Cyclic voltammograms of Ti/70%IrO_2-30%Ta_2O_5 electrode at $\nu = 20$ mV s^{-1} in 0.5 mol dm^{-3} H_2SO_4.

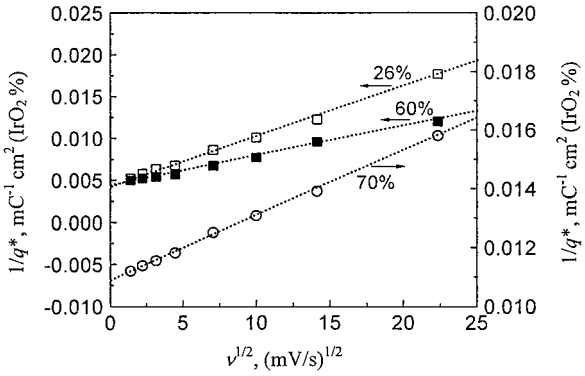

Figure 8 Extrapolation of q^* to $\nu = 0$ for various IrO_2 contents of IrO_2+Ta_2O_5 oxide electrodes: (- - -) linear region.

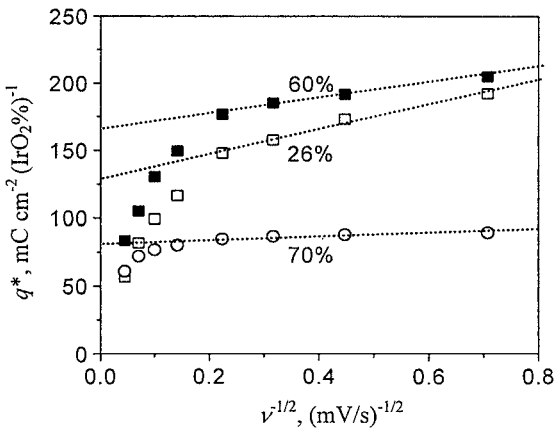

Figure 9 Extrapolation of q^* to $\nu = \infty$ for various IrO_2 contents of IrO_2+Ta_2O_5 oxide electrodes, (- - -) linear region.

drops in literatures [30] since the response current is much high at a high ν. Nevertheless, a satisfactorily linear region can be obtained at low scan rate region, which is plotted in the figure. Thus, $q^*(\nu = 0)$ and $q^*(\nu = \infty)$ can be evaluated, and q_i^* is easily determined by Equation 1.

The 'inner' and the 'outer' surface charge as well as the standard one, $q^*_{\nu=20}$, are showed in Fig. 10 as a function of oxide composition. The variations of q^* with IrO_2 content are much irregular. q^* oscillates with IrO_2 content, and the valley points occur at 10%, 40%, 70% and 100% IrO_2, respectively. The result of a relatively low value of q^* at 70% IrO_2 is not in agreement with the previous works reported by Comninellis *et al.* [5, 6]

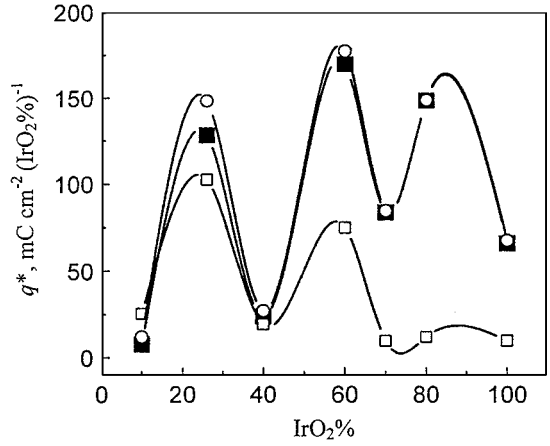

Figure 10 Dependence of q_i^* (□), q_s^* (■) and $q^*_{\nu=20}$ (○) on the composition of Ti/IrO_2-Ta_2O_5 oxide electrodes in 0.5 mol dm^{-3} H_2SO_4.

who found a maximum value of q^* at this composition. The reason for this difference is unclear, however, the different preparation process as described in the experimental details is the possible contribution. More details will be concerned in the further investigation. A low value for the sample of 10% IrO_2 is probably owing to the low activity at a low content of active component. And that for 100% IrO_2 indicates a positive effect of Ta component on active surface of the mixed oxide electrodes. As shown in Figs 2 and 3, the finest crystal grain has been found in both bulk and surface coating at 40% and 70% IrO_2. This seems that the low value of q^* is related to the fine crystallites of active component. However, according to the report of Brey and Davis [31], the total surface area of oxide films measured by BET (Brunauer, Emmet and Teller) nitrogen adsorption increases as the crystallite size is decreased. Further interpretation will be presented in the following context (see below). Fig. 10 also shows that q_i^* is extremely low at IrO_2 content of 70%, which indicates a much compact structure. It can be seen that, over the whole range of composition $q^*_{\nu=20}$ is more related to q_s^* than to q_i^* as shown from the curves.

3.4. Electrocatalytic activity

Potential-current curves are much featureless. Fig. 11 shows the variation of apparently normalized current

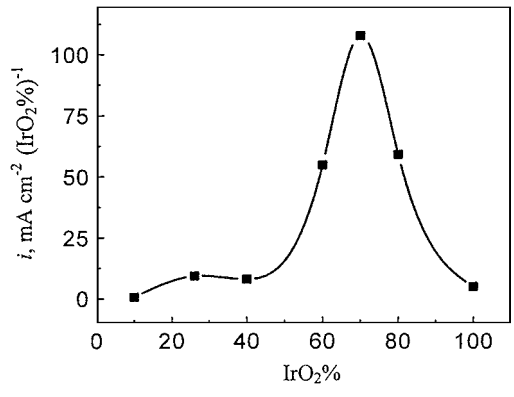

Figure 11 Normalized current for O_2 evolution at $E = 1.4$ V (SCE) on Ti/IrO_2-Ta_2O_5 anodes as a function of IrO_2 content in 0.5 mol dm^{-3} H_2SO_4 solution.

(denoted similarly as the normalized charge mentioned above) with oxide composition at $E = 1.4$ V (SCE). The current increases then decreases as the content of IrO_2 is increased, with a maximum at 70% IrO_2 which is contradictory to the results of voltammetric charges as shown in Fig. 10.

3.5. Double-layer capacitance

Little work on EIS has been done in the field of conductive metallic oxides [32, 33]. The results show that in both of 'double-layer' and OER potential regions the impedance data can be best fitted to $R_s(R_1C_1)(R_2C_2)L$ equivalent circuit, R_s is the resistance of solution between the reference and working electrodes. In this circuit the parallel (R_1C_1) combination has been related to Ir(III)/Ir(IV) transition processes occurring in the more internal, porous part of the oxide layer at a potential in 'double-layer' region, and to the physical properties of the film at a potential in OER region, respectively [32]. This combination makes a significant contribution to impedance data at low frequencies. The parallel (R_2C_2) combination takes account the surface transition processes occurring in the outer part of the oxide layer at 'double-layer' potentials, while is associated with the charge transfer processes of OER at high potentials, respectively [32]. This combination mainly affects the high-frequency part of impedance. The inductance, L, is probably resulted from the wiring and measuring equipment components. The typical magnitude of L is 1 μH obtained from the fitting results. Figs 12 and 13 shows the C_{dl} (C_2 in the circuit) values as a function of oxide composition at 0.7 and 1.35 V, respectively, As shown in Fig. 12 the value of C_{dl} oscillates with IrO_2 content, and the valley points occur at 10%, 40%, 70% and 100% IrO_2, respectively. This variation tendency is similar with that of integrated charge, q^*, as shown in Fig. 10. The value of double-layer capacitance of active electrodes is determined by the active reaction site number (ARSN) on the surface [32]. As stated above, large crystallite grains are segregated on the surface of 26% and 60% IrO_2 containing electrodes, coupling with wide grain boundaries which may be prone to the penetration of electrolyte into the inner layer and thus leads to an increase in measured q^* value. However, the C_{dl}~IrO_2% relationship changes dramatically at OER potentials. As shown in Fig. 13, during the oxygen

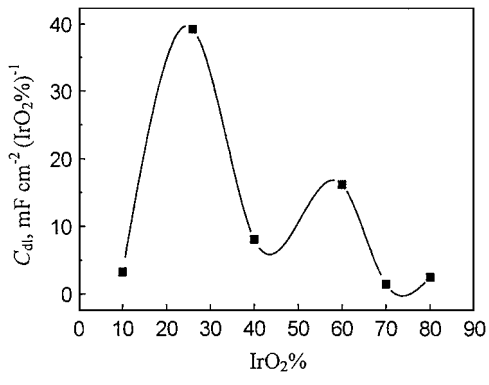

Figure 12 Double layer capacitance at 0.7 V (SCE) as a function of composition for IrO_2+Ta_2O_5 electrodes prepared at 450°C.

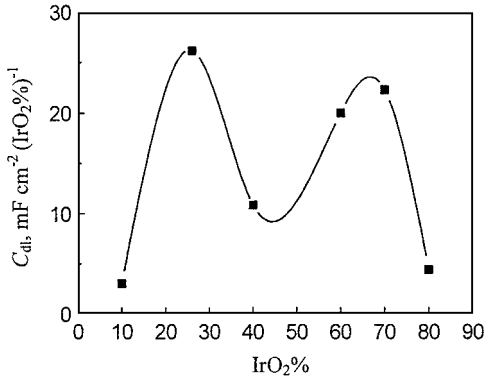

Figure 13 Double layer capacitance at 1.35 V (SCE) as a function of composition for IrO_2+Ta_2O_5 electrodes prepared at 450°C.

evolution the C_{dl} is increased for electrodes with the IrO_2 content higher than 40%. This indicates that the ARSN of IrO_2-Ta_2O_5 electrodes is enhanced after the surface modification by O_2 bubbling. The modification appears to be the most significant with the IrO_2 content 70% (compared with that at 0.7 V, C_{dl} increases 15 times). The decreasing of C_{dl} after oxygen evolution for low IrO_2 containing electrodes is probably associated with the low electrocatalytic activities.

4. Discussion

AT the steady state of open circuit, the potential of active oxide electrodes is determined by the surface transition redox [20, 26]. In the case of IrO_2 based oxides [30], the transition redox can be identified with the equilibrium:

$$2IrO_2 + 2H^+ + 2e^- \leftrightarrow Ir_2O_3 + H_2O \qquad (2)$$

This reaction is coincided with the value of $\partial E_{oc}/\partial pH$ of 0.06 V pH^{-1} derived from Fig. 6. The value of E_{oc} is thus expected to vary with the Ir^{IV}/Ir^{III} concentration ratio on surface. The highest E_{oc} of 70% IrO_2 containing mixed oxides indicates the highest value of $[Ir^{IV}]/[Ir^{III}]$ ratio for this composition. It has been widely accepted that, on metals [34, 35] and (or) oxides [36], the minimum required potential for oxygen evolution is determined by the metal/metal oxide or the lower metal oxide/higher metal oxide couple. For IrO_2 based oxide anodes, IrO_2/IrO_3 couple is generally concerned as the oxygen evolution governing couple [34, 36]. Since the concentration of Ir^{IV} component reaches the maximum value on the surface of Ti/70% IrO_2-30% Ta_2O_5, the equilibrium potential of IrO_2/IrO_3 couple is expected to be lowest, and the required potential for O_2 evolution is lowest at same time. Thus this anode is expected to present the highest electrocatalytic activity, which is in agreement with the current results shown in Fig. 7. The highest concentration of Ir^{IV} component in 70% IrO_2 containing electrodes may be related to the maximum solubilization between Ir and Ta oxides as indicated in 3.1.

However, it shold be noted that, this above determination is only based on the one hand. The voltammetric charge curves plotted in Fig. 10 show a much different (even some contradictory) tendency comparing with the current data shown in Fig. 11. To examine

the reliability of the charge data, C_{dl} obtained by EIS is measured. The results show that at a potential $E = 0.7$ V (in the 'double-layer' region for oxygen evolution), the variations of C_{dl} with the oxide compositions is very coincided with those of voltammetric charges (q_s^* and $q_{v=20}^*$). That is, C_{dl} and q^* can both determine the surface active sites of oxide electrodes in the 'double-layer' potential region. At an OER potential, however, the results change significantly. The C_{dl} of 40% and 70% IrO_2 containing oxide electrodes increases dramatically, while that of the other compositions is even decreased. Especially at 70% IrO_2 C_{dl} increases 15 times. This finding indicates that, in the case of intensive oxygen evolution, in which the electrode surface is attacked by the gas bubbling, the active surface sites of highly active electrodes tend to be increased. Combining with the results of structure and morphology measurements (see Section 3.1), it can be expected that the finer the crystal grains of the porous electrodes, the more the effect of the modification by the gas bubbling. Therefore, the highest electrocatalytic activity of 70% IrO_2 containing electrodes can, on the other hand, be interpreted by the finest crystalline of rutile which possesses significant surface modification to increase the active sites of oxides surface at a practical OER potential.

With the decrease of crystallite size, the pores, cracks and grain boundaries in surface tend to become smaller. Thus we assume that, resulting from the surface tension between solid and solution phases, the porous surface becomes less accessible to electrolyte penetration when the crystallite size is decreased, which results in decrease in the measured value of q^*. In the case of BET method, since the surface tension is relatively lower between solid and gas phases, the amount of gas absorption and adsorption increases with the decrease of grain size as a result of large number of boundaries. This assumption can probably explain the abnormal phenomenon of charge data in Fig. 10. During the oxygen evolution the number of 'real' active reaction sites tend to change with different surface morphology of oxide films.

It seems that the voltammetric charge, q^*, which is obtained at a relatively low potential (double-layer region for O_2 evolution) can not be preciously utilized to evaluate the real surface active site number of active oxides during practical O_2 evolution which is operated at a higher potential (OER region). The charge probably can only reveal the active are in the measured potential range. At a OER potential C_{dl} is a more suitable parameter in quantifying the 'real' surface active site number of electrodes since it is obtained by *in situ* EIS measurements.

5. Conclusions

1. The crystallization processes of two oxides in x $IrO_2 + (100 - x)$ Ta_2O_5 films affect each other. IrO_2 rutile exists as a solid solution of Ta component in IrO_2, and the solubility of Ta in rutile phase reaches the maximum value when $x = 70$ mol% at 450°C. Coatings with 40% and 70% IrO_2 present the finest crystallite grains on both the bulk and surface of oxide films.

2. A 'double-layer' electrochemical structure containing the 'inner' and 'outer' layers has been distinguished by cyclic voltammetry at varying potential scan rate and by EIS measurements. At 'double-layer' region potentials, both the voltammetric charge (q^*) and double layer capacitance (C_{dl}) appear to decline with the decrease of grain size of the bulk and surface coatings. However, the coatings of 70%IrO_2 + 30%Ta_2O_5 with the finest crystallites still exhibit the highest apparent activity for oxygen evolution evaluated by the current at a constant OER potential. The result can be attributed to two aspects. One is that the highest concentration of Ir^{IV} component exists on the coating surface at this composition shown from the highest open-circuit potential (E_{oc}), thus, the lowest initial potential for oxygen evolution is determined. And the other is that, as a result of the finest grains segregated on surface of 70% IrO_2 containing electrodes, large number of grain boundaries makes an intensive contribution to surface modification after attacked by oxygen bubbling at OER potentials, which leads to an increase in the total number of surface active reaction site.

3. The unconformity between q^* and current data shows that q^* obtained at a relatively low potential (in O_2 evolution double-layer region) can not be preciously utilized to evaluate the real surface active site number for practical O_2 evolution which is operated at a high potential (in OER region).

Acknowledgements

This work is subsidized by the Special Funds of the Chinese State Basic Research Projects (No. 19990650). The authors also gratefully acknowledge the financial support from China Postdoctoral Science Foundation and the Chinese State Key Laboratory for Corrosion and Protection.

References

1. H. B. BEER, US patent US549194 (1966); *Idem.*, US710551 (1968).
2. S. TRASATTI, *Electrochim. Acta* **45** (2000) 2377.
3. S. NIJJER, J. THONSTAD and G. M. HAARBERG, *ibid.* **46** (2001) 3503.
4. G. LODI, A. DE BATTISTI, G. BORDIN, C. DE ASMUNDIS and A. BENEDETTI, *J. Electroanal. Chem.* **277** (1990) 139.
5. C. COMNINELLIS and G. P. VERCESI, *J. Appl. Electrochem.* **21** (1991) 335.
6. J. ROLEWICZ, C. COMNINELLIS, E. PLATTINER and J. HINDEN, *Electrochim. Acta* **33** (1988) 573.
7. *Idem.*, *Chimia* **42** (1988) 75.
8. Y. E. ROGINSKAYA, O. V. MOROZOVA, E. N. LOUBNLN, A. V. POPOV, Y. I. ULITINA, V. V. ZHUROV, N. A. IVANOV and S. TRASSATI, *J. Chem. Soc. Faraday Trans.* **89** (1993) 1707.
9. Y. E. ROGINSKAYA and O. V. MORO ROZOVA, *Electrochim. Acta* **40** (1995) 817.
10. J. M. HU, H. M. MENG, J. Q. ZHANG, J. X. WU, D. J. YANG and C. N. CAO, *J. Mater. Sci. Lett.* **20** (2001) 1353.
11. F. CARDARELLI, P. TAXIL, A. SAVALL, CH. COMNINELLIS, G. MANOLI and O. LECLERC, *J. Appl. Electrochem.* **28** (1998) 245.
12. G. P. VERCESI, J. ROLEWICZ, C. COMNINELLIS and J. HINDEN, *Thermochim. Acta* **176** (1991) 31.

13. R. OTOGAWA, M. MORIMITSU and M. MATSUNAGA, *Electrochim. Acta* **44** (1998) 1509.
14. S. TRASATTI, "Electrodes of Conductive Metallic Oxides," Part A (Elsevier, Amsterdam, 1980).
15. R. BOGGIO, A. CARUGATI and S. TRASATTI, *J. Appl. Electrochem.* **17** (1987) 828.
16. L. A. DA SILVA, V. A. ALVES, S. C. DE CASTRO and J. F. C. BOODTS, *Colloids and Surfaces A: Physicochem. Eng. Aspects* **170** (2000) 119.
17. C. ANGELINETTA and S. TRASATTI, *Mater. Chem. Phys.* **22** (1989) 231.
18. S. PIZZINI and G. BUZZANCA, *Mater. Res. Bull.* **7** (1972) 449.
19. H. P. KLUG and L. E. ALEXAND, "X-Ray Diffraction Procedures for Polycrystalline and Amorphous Materials" (Wiley, New York, 1974).
20. Natl. Bur. Std. (U.S.) Mono. 25, Sec. 4 (1965).
21. L. L. XU, "The Semiconductor Fundamental of Oxides and Compounds" (Xi'an Electronic Science & Technology University Press, Xi'an, 1991) (in Chinese).
22. L. A. DE FARLA, J. F. C. BOODTS and S. TASATTI, *Electrochim. Acta* **37** (1992) 2511.
23. S. ARDIZZONE, A. CARUGATI and S. TRASATTI, *J. Electroanal. Chem.* **126** (1981) 287.
24. S. TASATTI, *Electrochim. Acta* **36** (1991) 225.
25. D. GALIZZIOLI, F. TANTARDINI and S. TRASATTI, *J. Appl. Electrochem.* **4** (1974) 52.
26. A. DE OLIVEIRA-SOUSA, M. A. S. DA SILVA, S. A. S. MACHADO, L. A. AVACA and P. DE LIMA-NETO, *Electrochim. Acta* **45** (2000) 4467.
27. L. D. BURKE and O. J. MURPHY, *J. Electroanal. Chem.* **96** (1979) 19.
28. S. ARDIZZONE, G. FREGONARA and S. TRASATTI, *Electrochim. Acta* **35** (1990) 263.
29. C. P. DE PAULI and S. TRASATTI, *J. Electroanal. Chem.* **396** (1995) 161.
30. D. BARONETTO, N. KRSTAJIC and S. TASATTI, *Electrochim. Acta* **39** (1994) 2359.
31. W. S. BREY and B. H. DAVIS, *J. Colloid and Interface Science* **70** (1979) 10.
32. L. A. DA SILVA, V. A. ALVES, M. A. P. DA SILVA, S. TRASATTI and J. F. C. BOODTS, *Electrochim, Acta* **42** (1997) 271.
33. V. A. ALVES, L. A. DA SILVA and J. F. C. BOODTS, *J. Appl. Electrochem.* **28** (1998) 889.
34. P. RASIYAH and A. C. C. TSEUNG, *J. Electrochem. Soc.* **131** (1984) 803.
35. A. HICKLING and S. HILL, *Discussions Faraday Society* **1** (1947) 236.
36. A. C. C. TSEUNG and S. JASEM, *Electrochim. Acta* **22** (1977) 31.

Received 29 April
and accepted 17 October 2002